LANGMUIR

pubs.acs.org/Langmuir Article

Diffusive Formation of Hollow Mesoporous Silica Shells from Core–Shell Composites: Insights from the Hydrogen Sulfide Capture Cycle of CuO@mSiO$_2$ Nanoparticles

Baoyue Fan, Wenyang Zhao, Supriya Ghosh, K. Andre Mkhoyan, Michael Tsapatsis,* and Andreas Stein*

Cite This: *Langmuir* 2020, 36, 6540–6549 Read Online

ACCESS | Metrics & More | Article Recommendations | Supporting Information

ABSTRACT: Mesoporous silica is often employed as a coating material in core–shell nanoparticles to decrease the possibility of sintering or aggregation of the core particles. In this work, we discovered a surprising morphological transformation during the sulfidation and regeneration (oxidation) of core–shell CuO@mSiO$_2$ materials designed for H_2S capture. Although CuS cores were still encapsulated within the silica shells after in situ sulfidation, hollow silica shells formed during the regeneration step as CuO leached out of the shell and aggregated into larger particles. The successful sulfidation of pristine CuO@mSiO$_2$ was facilitated by the restraining effect of silica shells on lattice growth from CuO into CuS, and the mesopores allowed for volume expansion. The phase and morphology changes during the regeneration (oxidation) process leading to the hollow shells were investigated by X-ray diffraction and transmission electron microscopy. It was observed that the cores remained encaged during the disproportionation of CuS to Cu_2S, which is the first step in the oxidation of CuS. However, voids were generated when Cu_2S was oxidized and reacted with water generated from the condensation of silica. A possible mechanism for this transformation involves the outward diffusion of copper ions through the mesoporous silica, leading to the migration of core particles. This migration was further accelerated by the elevated temperature in the regeneration process and promoted by the formation of the copper sulfate hydroxide through the reaction with water. This work provides key insights into the chemical stability of such core–shell structures under the influence of diffusion-driven structural transformations.

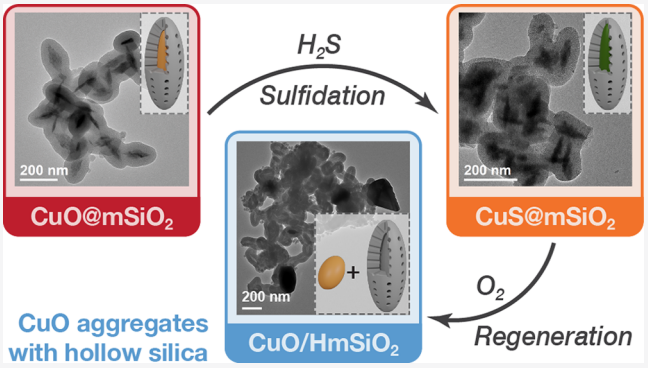

INTRODUCTION

Copper oxide has been extensively investigated for H_2S capture owing to its chemical affinity for H_2S.[1−6] In order to achieve reversible adsorption/desorption processes over multiple cycles, the sulfidation product, CuS, needs to be regenerated into copper oxide via a reaction with O_2. The two main steps in the H_2S adsorption process can be summarized as follows:

$$\text{Sulfidation: } CuO_{(s)} + H_2S_{(g)} \rightarrow CuS_{(s)} + H_2O_{(g)} \quad (1)$$

$$\text{Regeneration: } CuS_{(s)} + 3/2O_{2(g)} \rightarrow CuO_{(s)} + SO_{2(g)} \quad (2)$$

However, copper oxide nanoparticles tend to aggregate and sinter during the regeneration process at high temperatures, resulting in the loss of surface area and porosity. Therefore, an inert support is essential to improve the regenerability and structural stability of the active nanosized CuO particles.[7,8]

Core–shell composites have been widely studied in catalysis,[9−13] drug delivery,[14−19] and adsorption.[20−24] They are classified by the type of materials chosen for the inner and outer layers.[25] For our purpose, the shell material should be able to isolate the CuO particles and must remain structurally stable during the sulfidation and regeneration processes. In the past decades, silica has been developed as a common shell material due to two major advantages: it can increase the stability of the core nanoparticles, and it is relatively chemically inert.[26,27] In addition, if the silica shell is mesoporous (mSiO$_2$), the core particles remain accessible to guest species or reagents such as H_2S. A facile way to coat nanoparticles with mesoporous silica is the surfactant-templated sol–gel method.[28] In this method, a surfactant serves as a template to create mesopores by forming micelles on the surface of the

Received: April 3, 2020
Revised: May 18, 2020
Published: May 20, 2020

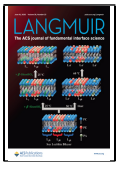

https://dx.doi.org/10.1021/acs.langmuir.0c00958
Langmuir 2020, 36, 6540–6549

nanoparticles, while a suitable silicon alkoxide undergoes hydrolysis on the surface under acidic or basic conditions and condenses around the micelles, creating a mesostructured layer. Finally, the surfactant template is removed through calcination or extraction to produce open mesopores. The uniformity and thickness of mesoporous silica shells can be tuned by adjusting the reaction pH and the reaction time. Mesoporous silica shells have been demonstrated to improve the stability of metal and metal oxide nanoparticles, such as Pt,[29,30] Au,[31,32] and Fe_3O_4.[14] The silica shells separate core particles from each other, thus mitigating nanoparticle aggregation. By virtue of the high surface area and large pore volume resulting from the mesopores, core@$mSiO_2$ nanoparticles are also excellent candidates for many catalytic[33,34] and biomedical applications.[14,18,19] Many of these previous studies have shown that mesoporous silica can be a beneficial shell material to stabilize core nanoparticles and maintain their morphology.

Core−shell composite structures may also be altered to create hollow structures through a subsequent intrananoparticle reaction.[35,36] Such a transformation is a combined result of ion diffusion in the core particle and structural confinement of the shell. The diffusion of ions may also result in the leaching of ions out of the nanoparticles. However, for core@$mSiO_2$ materials, very few studies have investigated the diffusion in mesoporous silica in depth. Although diffusive leaching of core ions through mesoporous silica in core−shell structures has been reported, it only occurred in a small fraction of particles and had minimal impact on the desired core−shell composite.[29]

In this study, core−shell CuO@$mSiO_2$ materials were synthesized and subjected to sulfidation−regeneration cycles for H_2S capture. During the regeneration process, we discovered the formation of hollow structures with mesoporous silica shells. Starting from CuO@$mSiO_2$ synthesized using the sol−gel method, we carried out in situ sulfidation of the copper oxide core and oxidative regeneration of the resulting copper sulfide. By exploring the morphology of the materials after the sulfidation and oxidation steps, we observed that the core−shell morphology was preserved during sulfidation but hollow silica shells were produced during oxidation. This unexpected morphology change led us to propose a possible mechanism for the formation of the hollow silica shells which involves the outward diffusion of copper ions and a series of other reaction steps. Our investigation into these transformations of CuO@$mSiO_2$ and CuS@$mSiO_2$ provides new insights into the stability of core−shell structures, especially when mesoporous silica serves as the coating material.

EXPERIMENTAL SECTION

Materials. All chemicals were used as received without further purification: copper(II) chloride dihydrate (crystalline certified) from Fisher Scientific; copper(II) nitrate trihydrate (ACS grade) from Sigma-Aldrich; cetyltrimethylammonium bromide (CTAB) and tetraethyl orthosilicate (TEOS, 98%) from Aldrich; sodium sulfide nonahydrate (ACS grade, 98%) from Alfa Aesar; sodium hydroxide pellets (ACS grade) from Avantor Performance Materials, Inc.; sulfuric acid (ACS grade, 95−98%) from VWR Chemicals BDH; ethanol (anhydrous, 200 proof) from Pharmco-AAPER. Deionized (DI) water produced on-site using a Milli-Q PLUS reagent-grade water system to a minimum resistivity of 18.2 MΩ·cm was used in all experiments.

Synthesis of Needlelike Core−Shell CuO@$mSiO_2$-N. The -N suffix indicates the needlelike shape of the core particles. Core−shell CuO@$mSiO_2$-N was synthesized by the following procedure. A mass of 100 mg of CTAB was dissolved in 50 mL of DI water to prepare a 5.5 mM CTAB solution. Then, 8.5 mg of $CuCl_2{\cdot}2H_2O$ was added. After the solution was heated to 70 °C, 200 μL of an aqueous 0.75 M NaOH solution was added while stirring, resulting in a pH between 10 and 11 for the reaction mixture. To create the mesoporous silica shell, 300 μL of 20% (v/v) TEOS in methanol was added dropwise to this mixture, three times (3 × 300 μL) in 30 min intervals. The resulting brown dispersion was maintained at 70 °C for 3 h with magnetic stirring at a rate of 600 rpm. The product was separated by centrifugation at 8000 rpm for 10 min and washed with ethanol. The centrifugation/washing procedure was repeated three times. To remove CTAB from the product, the as-synthesized CuO@$mSiO_2$-N was calcined in static air at 350 °C for 2 h in a tube furnace (heating ramp rate 2 °C/min).

In Situ Sulfidation of CuO@$mSiO_2$-N to Produce CuS@$mSiO_2$-N. A mass of 60 mg of $Na_2S{\cdot}9H_2O$ was placed at the bottom of a 15 mL centrifuge tube. A 2 mL vial containing 5 mg of calcined CuO@$mSiO_2$-N was also inserted into the centrifuge tube (Figure S1). To generate H_2S gas, 2 mL of 0.1 M H_2SO_4 was dropped into the centrifuge tube, reacting with Na_2S. Then the centrifuge tube was sealed immediately. After exposure to the H_2S atmosphere at room temperature for 24 h, the solid in the vial turned from brown to dark green, producing CuS@$mSiO_2$-N. (Caution: H_2S is toxic and flammable! This step must be performed in a functional fume hood, and the amounts of reagents should be limited. A safety data sheet for the handling of H_2S should be consulted before use.)

Regeneration of CuS@$mSiO_2$-N to Produce CuO/HmSiO_2-N. CuO with hollow silica shells (CuO/HmSiO_2-N) was prepared by calcining the CuS@$mSiO_2$-N sample obtained from the preceding step in static air in boat-shaped alumina crucibles in a tube furnace. The sample was calcined either by heating it gradually from room temperature to 600 °C at 5 °C/min and keeping it at that temperature for 6 h or placing the loaded crucible directly into a tube furnace that had already been preheated to 600 °C and keeping it there for 6 h. The resulting products were denoted as CuO/HmSiO_2-N1 and CuO/HmSiO_2-N2, respectively.

Synthesis of Dot-Shaped Core−Shell CuS@$mSiO_2$-D. The -D suffix indicates the dot shape of the core particles. Core−shell CuS@$mSiO_2$-D was synthesized following the previous literature.[37] A volume of 2 mL of 50 mM aqueous $CuCl_2$ solution was injected into 96 mL of 0.125 mg/mL aqueous CTAB solution. Then, 2 mL of 50 mM aqueous Na_2S solution was added dropwise under stirring, resulting in a golden-brown solution. After stirring for 15 min at 600 rpm, the solution was heated to 90 °C and maintained at 90 °C for 1 h under nitrogen flow. The solution turned dark green and contained CuS nanoparticles stabilized by CTAB (CuS−CTAB NPs). To coat the CuS−CTAB NPs with mesoporous silica shells, the solution was cooled to 70 °C, and 188 mg of CTAB was added to obtain a final CTAB concentration of 2 mg/mL (5.5 mM) in the reaction system. After several minutes of stirring, 700 μL of 2 M aqueous NaOH solution, 400 μL of TEOS, and 2 mL of ethyl acetate were rapidly added in sequence. The mixture was stirred at 70 °C for 30 min. The supernatant was separated by centrifugation at 12 000 rpm for 10 min. To precipitate the as-synthesized CuS@$mSiO_2$-D particles, the supernatant was split into four 25 mL fractions, and 15 mL of ethanol was added into each fraction of the supernatant. The product was separated by centrifugation at 12 000 rpm for 10 min and washed with ethanol twice more at 12 000 rpm for 5 min.

Calcination of CuS@$mSiO_2$-D to Produce CuO/HmSiO_2-D. The CuS@$mSiO_2$-D sample obtained from the preceding step was first pyrolyzed using a boat-shaped alumina crucible in a tube furnace at 350 °C for 30 min under nitrogen, followed by calcination in static air at 600 °C for 6 h in a tube furnace with a continuous heating ramp rate of 5 °C/min. CuO with hollow silica shells (CuO/HmSiO_2-D) was produced.

To study the phase and morphology changes during the pyrolysis/calcination process, intermediate CuS@$mSiO_2$-D samples were

https://dx.doi.org/10.1021/acs.langmuir.0c00958
Langmuir 2020, 36, 6540−6549

Scheme 1. Schematic Illustration of Mesoporous Silica Coating on Needlelike CuO Nanoparticles

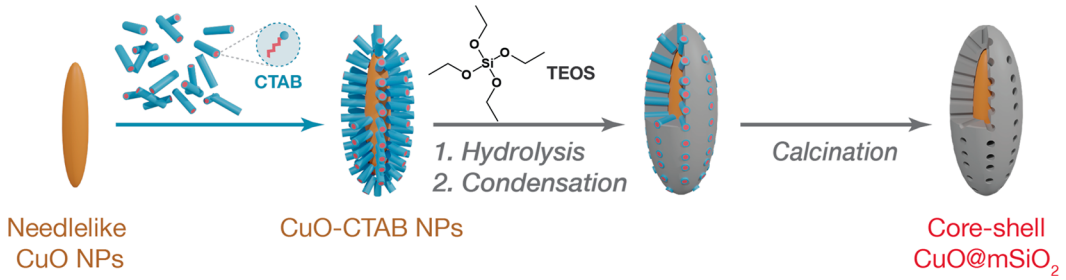

collected once the temperature reached 250, 350, and 450 °C in the process above. These were denoted as CuS@mSiO$_2$-D-250/350/450, respectively.

Characterization. Powder X-ray diffraction patterns were collected using an X'Pert Pro diffractometer with a Co Kα radiation source (λ = 1.789 Å) operating at 45 kV and 40 mA. Grain sizes were calculated using the Scherrer equation. FT-IR spectroscopy was performed on a Nicolet Magna-FTIR 760 spectrometer using KBr pellets of the samples. Transmission electron microscopy images were acquired on a FEI Tecnai T12 microscope operating at 120 kV accelerating voltage. Scanning transmission electron microscopy (STEM) was performed on an aberration-corrected FEI Titan G^2 microscope operating at an accelerating voltage of 200 kV. Energy-dispersive X-ray spectroscopy (EDS) elemental maps were collected using a SuperX EDS detector. The TEM samples were prepared by dispersing the nanoparticles in ethanol and bath sonicating for about 15 min. Formvar-coated Cu grids were dipped into the suspension and dried.

RESULTS AND DISCUSSION

Mesoporous Silica Coating on CuO Nanoparticles. Unprotected H_2S sorbents based on CuO nanoparticles experience extensive grain growth and aggregation after multiple sulfidation and regeneration cycles (Figure S2). The original motivation for this work was, therefore, to investigate the utility of mesoporous silica coatings to stabilize CuO nanoparticles under such reactive conditions. Needlelike CuO nanoparticles were coated with mesoporous silica by the procedure illustrated in Scheme 1. TEOS, the silica precursor, was hydrolyzed under basic conditions to produce the silica shells. The surfactant CTAB served as the capping reagent to stabilize the needlelike CuO nanoparticles. It was also used as the organic template for the mesoporous silica shells.[28]

The powder XRD pattern of CuO@mSiO$_2$-N (Figure 1a) matched the reflections of CuO and indicated that this phase was highly crystalline. The peak at 2.5° 2θ in the low-angle XRD pattern was attributed to (100) reflections of mesoporous silica, from which the average mesopore repeat unit in the shell was determined to be approximately 4 nm. The mesoporous silica shell was also responsible for the broad peak between 20 and 30° 2θ. TEM images of CuO@mSiO$_2$-N (Figure 1b) showed that needlelike CuO particles were encapsulated by mesoporous silica shells and remained so after calcination (Figure 1c, Figure S3). The average thickness of the silica shells (39 ± 3 nm) and particle width (103 ± 9 nm) were also maintained after calcination (Figure S4a–d). The lengths of the needlelike CuO cores ranged from 60 to 120 nm, and their widths from 10 to 20 nm.

FTIR spectra of CuO@mSiO$_2$-N before and after calcination (Figure 2) show the expected features of the mesoporous silica shells. The absorption peaks at 1080 and 798 cm^{-1} correspond to the symmetric and asymmetric stretching vibrations of the Si–O–Si bonds. The peaks at 964 and 461 cm^{-1} correspond to Si–OH stretching and Si–O bending vibrations, respectively.[38] The absorption bands at around 3200 and 1460 cm^{-1} are assigned to –OH groups and adsorbed water molecules. The bands at about 2900 and 1480 cm^{-1} are due to C–H vibrations from the surfactant template. After calcination at 350 °C, the intensity of C–H bands decreased significantly, confirming the removal of most CTAB molecules.

Effects of In Situ Sulfidation on the Core–Shell Structure. A complete conversion of the cores in CuO@mSiO$_2$-N from CuO to CuS was achieved after 24 h exposure to an H_2S atmosphere, as confirmed by the powder XRD patterns in Figure 3a. The average grain size of the sulfidated core was estimated to be 21 nm from the XRD patterns; i.e., the grain size did not change compared with the as-synthesized 21 nm CuO particles in the original core–shell structure (CuO@mSiO$_2$-N-calcined). A selected-area electron diffraction (SAED) pattern (Figure 3d) confirmed that the resulting cores consisted of CuS (PDF# 00-006-0464). TEM images in Figure 3b and 3c show that in core–shell CuS@mSiO$_2$-N, CuS still maintained a needlelike shape and remained encapsulated in the mesoporous silica shell. No isolated CuS particles were observed. Previous studies demonstrated successful preservation of the original core shape in core–shell Pt@mSiO$_2$ after heat treatment as the silica shell prevented the aggregation of metal nanoparticles.[29] Our results indicate that mesoporous silica shells help to maintain the shape of the cores even after certain chemical reactions.

We also noticed that the surfaces of the CuS cores in core–shell CuS@mSiO$_2$-N (Figure 3c) were not as smooth as the CuO cores in the precursor material (Figure S3). The widths of the encapsulated CuS cores increased to 26 ± 5 nm compared to the widths of the original needlelike CuO cores (17 ± 4 nm, Figure S7). A possible reason for the expanded sizes is the lattice difference between CuO and CuS (Table 1) because the unit cell volume normalized by the number of Cu atoms in the unit cell (V/Z) increased from 20 to 34 Å^3. In addition, on the basis of image contrast, the average thickness of the silica shells apparently decreased to 34 ± 3 nm after sulfidation (Figure S4e) when compared with the original silica shells (40 ± 3 nm) in CuO@mSiO$_2$-N-calcined (Figure S4c). The average particle width of CuO@mSiO$_2$-N-calcined was 103 ± 10 nm, and that of CuS@mSiO$_2$-N was 102 ± 10 nm (Figure S4d, f). The unchanged particle width combined with the apparent decrease in shell thickness indicated that some copper ions diffused into the mesopores when the pristine CuO reacted with the inward moving H_2S gas, increasing the image contrast in those parts of the mesopores. These observations further indicated that the mesopores in silica played a key role in keeping the initial needlelike core shape in

https://dx.doi.org/10.1021/acs.langmuir.0c00958
Langmuir 2020, 36, 6540–6549

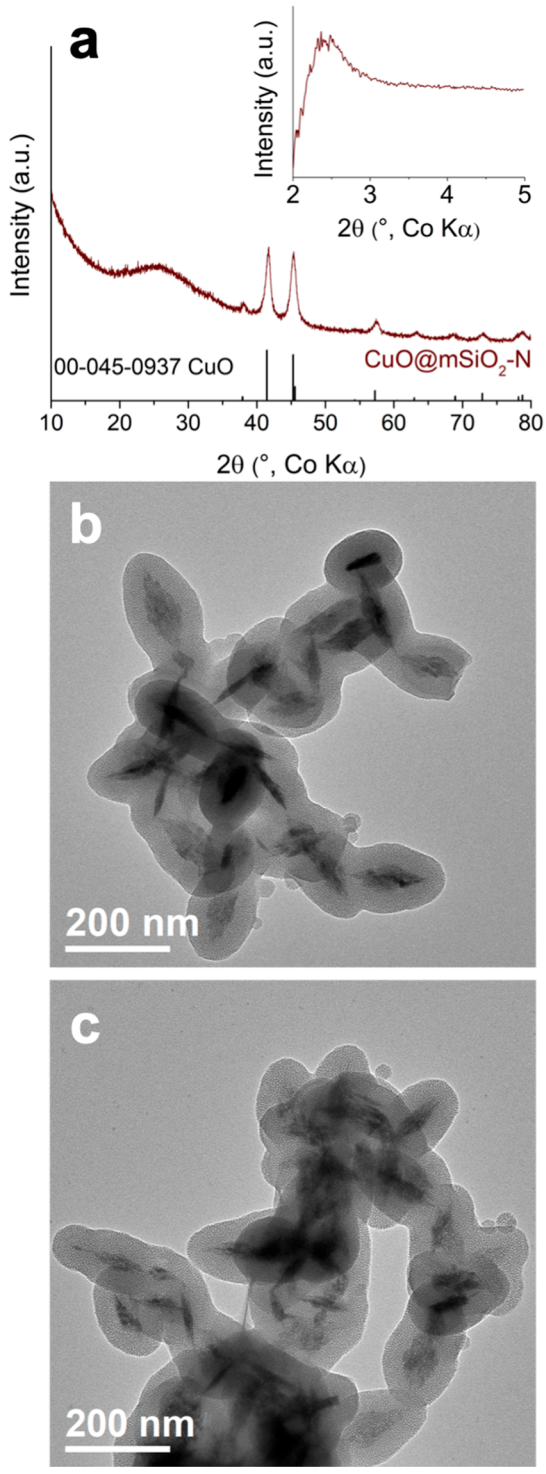

Figure 1. (a) XRD pattern of CuO@mSiO$_2$-N (see Figure S5 for an enlarged version). TEM images of CuO@mSiO$_2$-N (b) before and (c) after calcination. The inset in (a) is the low-angle XRD pattern. The -N suffix indicates the needlelike shape of the core particles.

the core−shell structure, allowing for the volume expansion when the core composition changed from CuO to CuS during the sulfidation.

Formation of Hollow Silica Shells after Regeneration. As noted above, silica shells are generally employed to preserve the core shapes in core−shell structures and prevent cores from aggregating.[29] Surprisingly, a typical TEM image of the

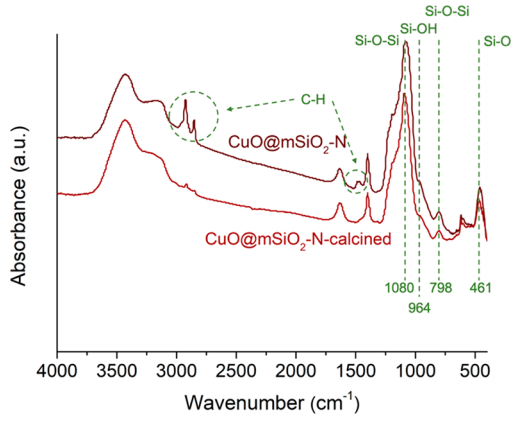

Figure 2. FTIR spectra of CuO@mSiO$_2$-N and CuO@mSiO$_2$-N-calcined at 350 °C.

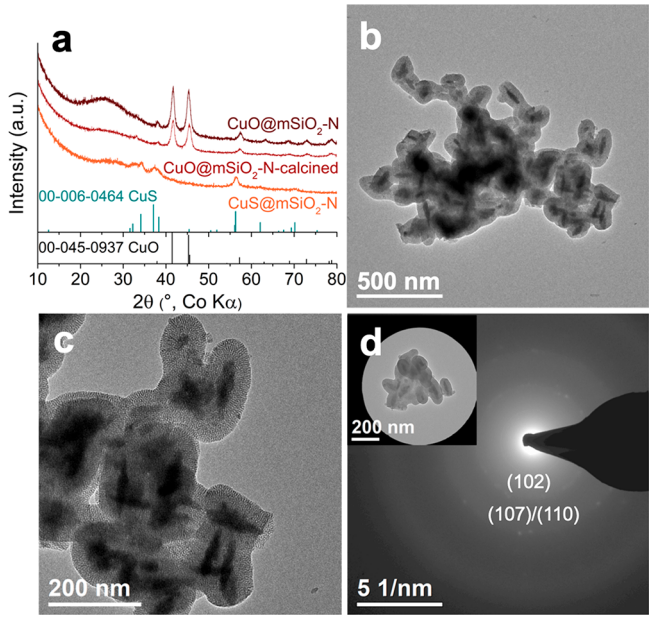

Figure 3. (a) Powder XRD patterns of CuO@mSiO$_2$-N before and after calcination in air at 350 °C and of the sulfided material CuS@mSiO$_2$-N (see Figure S6 for an enlarged version). TEM images at (b) low and (c) high magnifications and (d) SAED pattern of sulfidated core−shell CuS@mSiO$_2$-N. Reflections in (d) match those of CuS (PDF# 00-006-0464). The inset in (d) shows the region from which the SAED pattern was taken.

Table 1. Crystal Structure Data of CuO and CuS[39]

phase (PDF#)	CuO (00-045-0937)	CuS (00-006-0464)
space group	*C*2/*c* (monoclinic)	*P*63/*mmc* (hexagonal)
Z	4	6
unit cell volume (Å^3)	81.2	203.5
V/*Z* (Å^3)	20	34

regenerated sample obtained by calcination of needlelike core−shell CuS@mSiO$_2$-N1 (Figure 4a) showed hollow silica shells, along with some large particles on the outside (Figure 4b). The SAED pattern of one of these external particles (Figure 4c) matched the reflections of CuO, showing that the copper species escaped through the mesoporous shell during the regeneration process.

More interestingly, if CuS@mSiO$_2$-N was directly placed into a preheated furnace at 600 °C (CuO/HmSiO$_2$-N2), some

https://dx.doi.org/10.1021/acs.langmuir.0c00958
Langmuir 2020, 36, 6540−6549

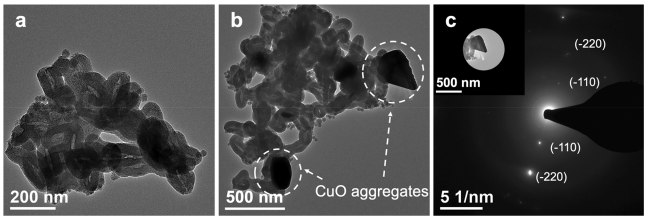

Figure 4. (a, b) TEM images and (c) SAED pattern of CuO/$HmSiO_2$-N1. Reflections in (c) match those of CuO (PDF# 00-045-0937). The inset in (c) shows the region of the sample from which the SAED pattern was obtained.

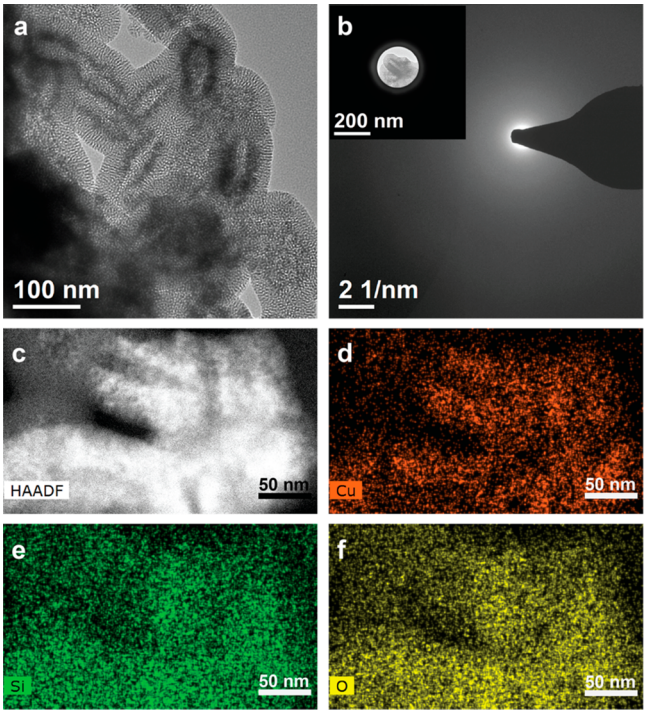

Figure 5. (a) TEM image, (b) SAED pattern, and (c–f) high-angle annular dark-field (HAADF) STEM image of CuO/$HmSiO_2$-N2, and the corresponding STEM-EDS elemental maps for Cu, Si, and O.

dark residues were found in the bright-field TEM image around the core of the core–shell structures (Figure 5a). However, no crystalline phase was identified in the SAED pattern (Figure 5b), and the residue consisted mostly of copper on the basis of STEM-EDS elemental maps (Figure 5c–f). Very little sulfur was present according to the low EDS signal, which was in the range of instrumental noise (Figure S8).

Mesoporous Silica Coating on CuS Nanoparticles. To investigate the formation of hollow silica shells during the regeneration process, CuS@$mSiO_2$-D was directly synthesized via the sol–gel method (Scheme 2).

The XRD pattern of CuS@$mSiO_2$-D in Figure 6a gives evidence for the formation of CuS with low crystallinity. Similar to that of CuO@$mSiO_2$-N, the low-angle XRD pattern shows a peak at 2.5° 2θ that is attributed to the (100) reflections of mesoporous silica with an average repeat unit of approximately 4 nm. As seen in the TEM images of CuS@$mSiO_2$-D (Figure 6b–d), most dot-shaped CuS particles were coated by the mesoporous silica shells. Not all CuS dots were located at the center of the particles, and some particles

Scheme 2. Schematic Illustration of the Formation Process of Core–Shell CuS@$mSiO_2$ by Coating Mesoporous Silica onto Dot-Shaped CuS Nanoparticles

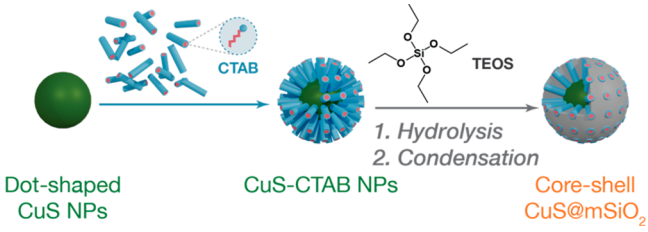

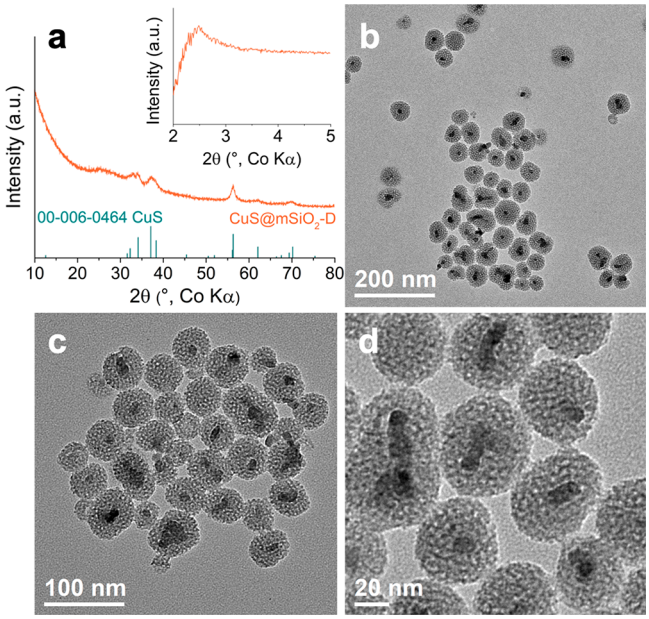

Figure 6. (a) XRD pattern and (b–d) TEM images of CuS@$mSiO_2$-D at different magnifications. The inset in (a) is the low-angle XRD pattern. The -D suffix indicates the dot shape of the core particles. An enlarged version of the XRD patterns is provided in Figure S11.

contained more than one CuS dot. The average thickness of the silica shells was around 16 ± 2 nm (Figure S9), and the diameter of the CuS cores was 10–15 nm. An FT-IR spectrum also confirmed the presence of silica in the composite nanoparticles (Figure S10). At this stage, mesopores were still occupied by surfactant, as seen by the IR peaks originating from the C–H stretching modes. After calcination of these materials to remove the surfactant and oxidize the cores, similar hollow shells were observed as for CuO/$HmSiO_2$-N but with spherical voids in the case of CuO/$HmSiO_2$-D (Figure 7a–b). Large external CuO aggregates were found and identified by SAED (Figure 7c).

Phase and Morphology Changes during Regeneration. To investigate the reason why hollow silica particles were produced during the regeneration, the phase and morphology changes during the calcination process of CuS@$mSiO_2$-D were studied by sampling intermediate products at different temperatures. The powder XRD patterns in Figure 8 provide information about the intermediate phases as the CuS cores were oxidized at different temperatures in the calcined samples.

Cubic Cu_2S (PDF# 00-002-1284) was observed in the XRD pattern of CuS@$mSiO_2$-D that had been calcined at 250 °C. Cu_2S was produced by the disproportionation of CuS as shown

https://dx.doi.org/10.1021/acs.langmuir.0c00958
Langmuir 2020, 36, 6540–6549

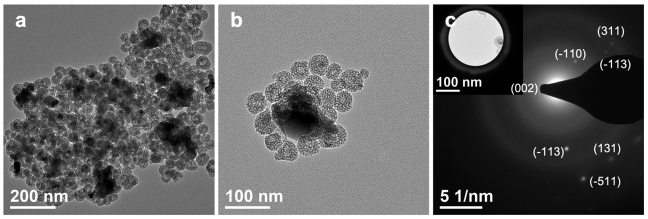

Figure 7. (a, b) TEM images and (c) SAED pattern of CuO/$HmSiO_2$-D. Reflections in (c) match those of CuO (PDF# 00-045-0937). The inset in (c) shows the sample region from which the SAED pattern was obtained.

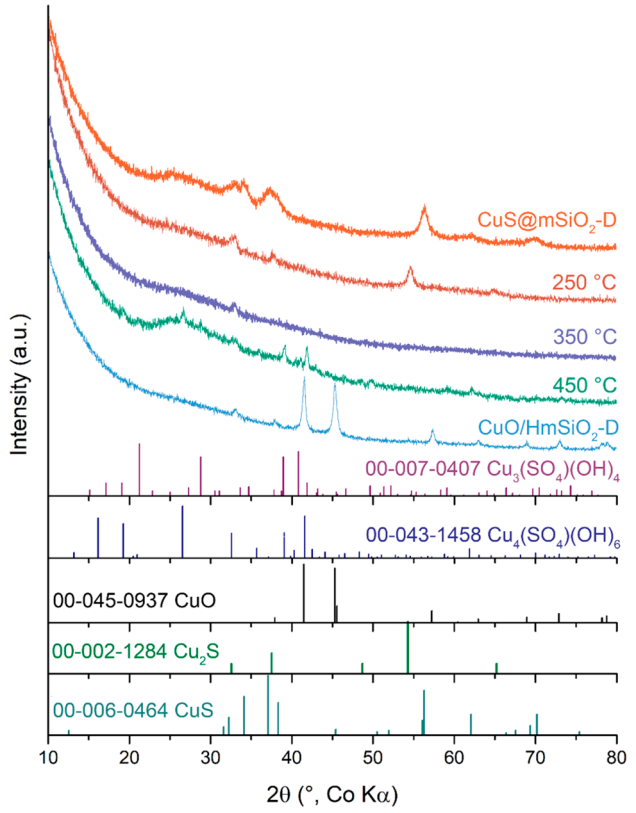

Figure 8. Powder XRD patterns of CuS@$mSiO_2$-D calcined at different temperatures. The small peak at 33.1° 2θ is attributed to the (111) reflection of silicon from the sample holder (PDF# 00-027-1402).

in reaction 3 below. The sulfur byproduct was observed by SAED (Figure S12) as an S_8 phase (PDF# 00-053-1109) at 350 °C before the atmosphere was switched from N_2 to O_2. In the presence of O_2, as the temperature was increased, sulfur could be further oxidized to SO_2. At 350 °C, no bulk crystalline phase was found. Then, copper sulfate hydroxide phases $Cu_3(SO_4)(OH)_4$ (PDF# 00-007-0407) and $Cu_4(SO_4)(OH)_6$ (PDF# 00-043-1458) formed at 450 °C following reactions 4 and 5. Subsequently, the copper sulfate hydroxides decomposed (reactions 6 and 7) and finally produced CuO at 600 °C (reaction 8). In a previous study by Kundu and Pradham on the thermal oxidation of bulk CuS, similar intermediate phases (Cu_2S and copper sulfate hydroxides) were observed.[40] However, these intermediates and CuO were produced at lower temperatures in our study. The likely cause for the lower conversion temperatures is the fact that the 20 nm cores of the CuS synthesized here were smaller than the particles in the previous study by 2 orders of magnitude. On the basis of the intermediates observed during the calcination, the proposed reaction sequence for the oxidation mechanism is summarized as follows:[40]

$$2CuS_{(s)} \rightarrow Cu_2S_{(s)} + \frac{1}{x}S_{x(l)} \quad (3)$$

$$2Cu_2S_{(s)} + 5O_{2(g)} + 2H_2O_{(g)} \rightarrow Cu_3(SO_4)(OH)_{4(s)} + CuSO_{4(s)} \quad (4)$$

$$3Cu_2S_{(s)} + 7.5O_{2(g)} + 3H_2O_{(g)} \rightarrow Cu_4(SO_4)(OH)_{6(s)} + 2CuSO_{4(s)} \quad (5)$$

$$Cu_3(SO_4)(OH)_{4(s)} \rightarrow Cu_2OSO_{4(s)} + CuO_{(s)} + 2H_2O_{(g)} \quad (6)$$

$$Cu_4(SO_4)(OH)_{6(s)} \rightarrow Cu_2OSO_{4(s)} + 2CuO_{(s)} + 3H_2O_{(g)} \quad (7)$$

$$Cu_2OSO_{4(s)} \rightarrow 2CuO_{(s)} + SO_{2(g)} + 0.5O_{2(g)} \quad (8)$$

Although no crystalline $CuSO_4$ or Cu_2OSO_4 phases were observed in our study, perhaps due to very small grain sizes, such phases were seen in the study by Kundu and Pradham,[40] so it is reasonable to assume that reactions 4–8 were also operative in our work.

TEM images (Figure 9, Figure S13) were acquired for the samples calcined at 250 and 350 °C. The core–shell structures were maintained at 250 °C, and the Cu_2S cores remained encapsulated in the silica shells. Hence, the disproportionation of CuS (reaction 3) did not affect the morphology of the core–shell structure. However, hollow silica particles appeared in the sample calcined at 350 °C, which indicated that the leaching of core particles accompanied reactions 4 and 5.

Moreover, interconnected nanoparticles bridged by smaller particles were observed in the CuS@$mSiO_2$-D-350 sample (Figure 10a–b). STEM-EDS elemental maps (Figure 10c–h) showed the presence of both Cu and S signals in the bridging particles. These two elements were also located in the silica shells. Cu and S elemental distributions provided evidence that the core particles formed connections with the neighboring cores as they diffused out and finally formed external aggregates. In this case, mesoporous silica shells were not able to protect the core–shell morphology in the oxidation process of Cu_2S. This phenomenon indicated that the interfacial energy between the core and silica shell is higher than the total surface energies of the inner surface of silica and the external aggregated core material.

Proposed Mechanism for the Formation of Hollow Shells. The formation of hollow structures has been widely studied in a number of processes, including the sulfidation of metal oxides,[41] oxidation of metals,[42] and oxidation of metal sulfides.[43] The generation of voids is usually explained by the Kirkendall effect for cases in which the outward diffusion of ions is faster than the inward diffusion of gases.[44–46] Nevertheless, existing studies have only addressed the case where a single-component material reacts directly with the inward diffusing gas. In our core–shell structured composites, both incoming gas and outward diffusing species have to pass through the mesoporous silica shells.

Here, we propose a possible mechanism for the formation of hollow silica shells during the oxidation of copper sulfide

https://dx.doi.org/10.1021/acs.langmuir.0c00958
Langmuir 2020, 36, 6540–6549

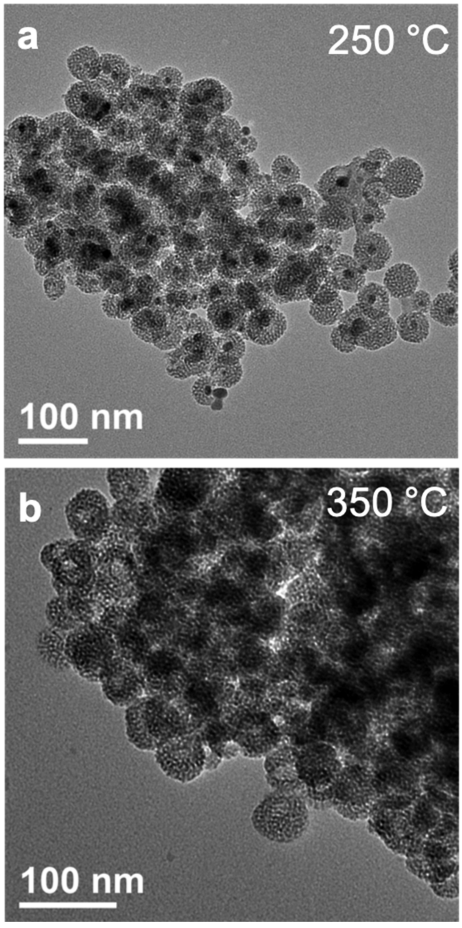

Figure 9. TEM images of (a) CuS@mSiO$_2$-D-250 and (b) CuS@mSiO$_2$-D-350.

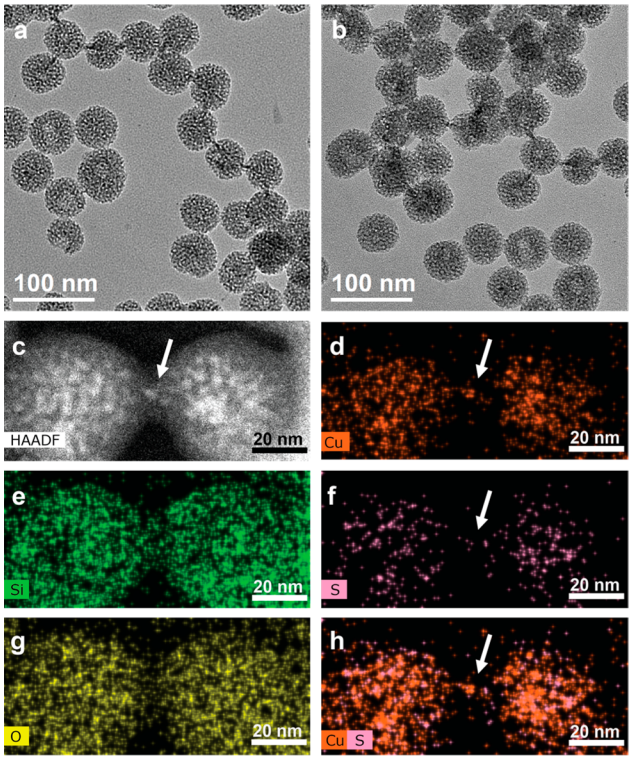

Figure 10. (a, b) TEM images of the "linked particles" observed in CuS@mSiO$_2$-D-350. (c–h) HAADF-STEM image of two linked particles in CuS@mSiO$_2$-D-350 with STEM-EDS elemental maps for Cu, Si, S, and O and an overlay of the Cu and S maps. The arrows show the bridge between the linked particles.

(Scheme 3). In contrast to diffusion in elemental metal nanoparticles where only one species is involved, both metal cations and sulfide anions may contribute to ion diffusion in sulfides. However, due to the differences in ionic radii, copper ions are more likely than sulfide ions to diffuse through the lattice[47] via a vacancy mechanism.[48,49] Although it has been reported that the copper ions in copper films tend to diffuse out through silica,[50] no studies have investigated such diffusion processes through silica from copper sulfides. Our study revealed that the copper ions in copper sulfides have a high tendency to diffuse out through the silica shell. Thermadam et al. demonstrated that a temperature increase accelerates the diffusion of the copper ions from a copper film through silica.[50] In our study, during the process of regeneration, the elevated temperature likely facilitates the copper ion diffusion from copper sulfide nanoparticles into silica shells.

In the H_2S adsorption cycle with CuO@mSiO$_2$ nanoparticles, the leaching and aggregation of copper ions only occurred during the regeneration step, whereas the core–shell structure remained intact after sulfidation. Therefore, another question is whether there are other driving forces for the outward diffusion of copper ions. Nguyen et al. studied a chemical system where bimetal core–shell Cu@Ni particles undergo phosphidation.[51] In their study, the core Cu moved out from the original core–shell structure of Cu–Ni and formed large aggregates of Cu during the phosphidation process. The authors proposed that the formation of Cu–P species was a driving force for outward copper diffusion. A main implication of both their results and our observations is that chemical reactions taking place in the shell further decrease the ion concentration near the shell and thereby promote the diffusion of core ions.

In our proposed regeneration reaction sequence involving CuS@mSiO$_2$, the disproportionation of copper(II) sulfide into copper(I) sulfide and sulfur (reaction 3) did not involve any outside reactants; therefore, the reaction did not change the core–shell structure. Then, hollow silica shells were generated when copper(I) sulfide was further oxidized to copper sulfate hydroxides through reactions 4 and 5, which require participation of water molecules. As the temperature was increased during regeneration, water molecules may have been produced from condensation of hydroxyl groups in the silica shells. Hence, the formation of copper sulfate hydroxides may further promote the displacement of copper ions from the center of the core–shell structure and their outward diffusion through the mesoporous silica shell. This is also evident from the presence of copper-containing species in the core–shell structure (Figure 5a) when the furnace was preheated at 600 °C. Compared with the lower temperature of 350 °C when the hollow silica shells were first observed, the greater tendency for silica condensation at 600 °C increased the production of water and thus the probability of water molecules moving into the center of the core–shell structure and reacting with copper sulfides. Hence, the water molecules were able to participate in reactions 4 and 5 before all copper ions diffused out from the center, resulting in the copper-containing residue left in the center.

https://dx.doi.org/10.1021/acs.langmuir.0c00958
Langmuir 2020, 36, 6540–6549

Scheme 3. Schematic Illustration of the Proposed Mechanism for the Formation of Hollow Silica Shells from Core−Shell CuS@mSiO$_2$

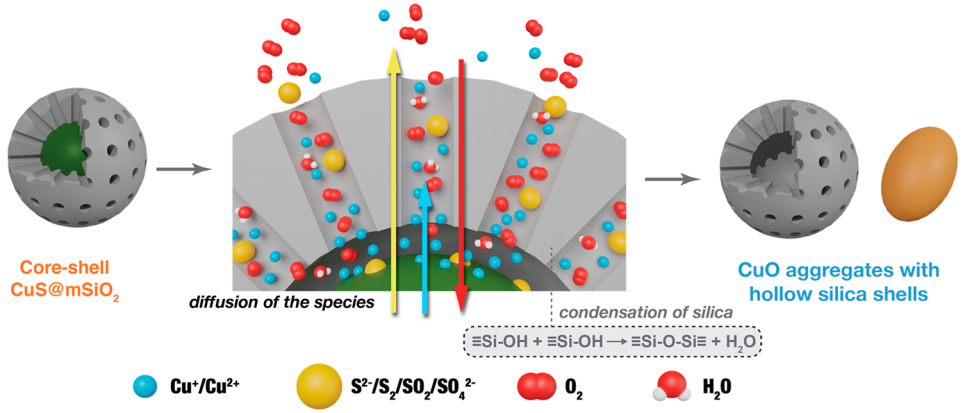

CONCLUSION

In this work, core−shell structures of needlelike CuO coated by mesoporous silica (CuO@mSiO$_2$) were synthesized and subjected to a sulfidation−regeneration cycle for H_2S capture as a potential application. After the core−shell particles were exposed to an H_2S atmosphere during in situ sulfidation, the CuO was fully converted to CuS while the core−shell structure was maintained because the mesopores allowed for volume expansion from copper oxide into copper sulfide. In contrast, oxidation of core−shell CuS@mSiO$_2$ led to the formation of hollow silica shells and large aggregates of CuO outside the silica. On the basis of the observed phase and morphology changes during the oxidation process, a possible mechanism was proposed for the generation of voids in the center of the mesoporous silica shells. The outward diffusion of copper ions through mesoporous silica caused the migration of core particles, which was accelerated by an increase in temperature and promoted by the production of copper sulfate hydroxides via reactions with water from the condensation of the silica.

This study provides new insights into the chemical behavior of mesoporous silica shells in applications of core−shell nanoparticles. The shells may protect nanoparticles from aggregating and, at the same time, offer access to the inner cores, as many studies have shown. Yet our discoveries reveal the possibility of outward diffusion of the inner core material, especially when the diffusion is facilitated by elevated temperatures or chemical reactions taking place. Similar chemical transformations may also apply for other core−shell structures and can provide new routes for the development of novel nanoparticle structures. Our findings can also guide the performance optimization of silica-shell-encapsulated nanoparticles targeted for adsorptive separation, catalytic applications, or sensing, where the chemical environment of the inert silica shell and the interactions between core and shell play a vital role in determining the activity and stability of such nanoparticles over multiple operational cycles. Future studies will focus on the possible role of porosity and pore size[52] in the shell to modulate the diffusion of core materials and sorbates.

ASSOCIATED CONTENT

Supporting Information

The Supporting Information is available free of charge at https://pubs.acs.org/doi/10.1021/acs.langmuir.0c00958.

Experimental setup for in situ sulfidation, additional TEM images, size histograms, STEM elemental maps, and FT-IR spectra (PDF)

AUTHOR INFORMATION

Corresponding Authors

Andreas Stein − *Department of Chemistry, University of Minnesota, Minneapolis, Minnesota 55455, United States;* orcid.org/0000-0001-8576-0727; Email: a-stein@umn.edu

Michael Tsapatsis − *Department of Chemical and Biomolecular Engineering & Institute for NanoBioTechnology, Johns Hopkins University, Baltimore, Maryland 21218, United States;* orcid.org/0000-0001-5610-3525; Email: tsapatsis@jhu.edu

Authors

Baoyue Fan − *Department of Chemistry, University of Minnesota, Minneapolis, Minnesota 55455, United States*

Wenyang Zhao − *Department of Chemistry, University of Minnesota, Minneapolis, Minnesota 55455, United States;* orcid.org/0000-0002-0828-3813

Supriya Ghosh − *Department of Chemical Engineering & Materials Science, University of Minnesota, Minneapolis, Minnesota 55455, United States*

K. Andre Mkhoyan − *Department of Chemical Engineering & Materials Science, University of Minnesota, Minneapolis, Minnesota 55455, United States;* orcid.org/0000-0003-3568-5452

Complete contact information is available at: https://pubs.acs.org/10.1021/acs.langmuir.0c00958

Notes

The authors declare no competing financial interest.

ACKNOWLEDGMENTS

This work was partially supported by the Gas Sub-Committee R&D arm of the Abu Dhabi National Oil Company United Arab Emirates and partially by funding from the Industrial Partnership for Research in Interfacial & Materials Engineering at the University of Minnesota. Parts of this work were carried out in the Characterization Facility, University of Minnesota, which receives partial support from the NSF through the MRSEC program. The authors thank Professor R. L. Penn for use of the powder X-ray diffractometer.

REFERENCES

(1) Laperdrix, E.; Costentin, G.; Saur, O.; Lavalley, J. C.; Nédez, C.; Savin-Poncet, S.; Nougayrède, J. Selective Oxidation of H_2S over CuO/Al_2O_3: Identification and Role of the Sulfurated Species Formed on the Catalyst during the Reaction. *J. Catal.* **2000**, *189*, 63−69.

(2) Ko, T. H.; Chu, H.; Chaung, L. K. The Sorption of Hydrogen Sulfide from Hot Syngas by Metal Oxides over Supports. *Chemosphere* **2005**, *58*, 467−474.

(3) Montes, D.; Tocuyo, E.; González, E.; Rodríguez, D.; Solano, R.; Atencio, R.; Ramos, M. A.; Moronta, A. Reactive H_2S Chemisorption on Mesoporous Silica Molecular Sieve-Supported CuO or ZnO. *Microporous Mesoporous Mater.* **2013**, *168*, 111−120.

(4) Rodriguez, J. A.; Jirsak, T.; Chaturvedi, S. Reaction of H_2S with MgO(100) and Cu/MgO(100) Surfaces: Band-Gap Size and Chemical Reactivity. *J. Chem. Phys.* **1999**, *111*, 8077−8087.

(5) Xue, M.; Chitrakar, R.; Sakane, K.; Ooi, K. Screening of Adsorbents for Removal of H_2S at Room Temperature. *Green Chem.* **2003**, *5*, 529−534.

(6) Liu, D.; Chen, S.; Fei, X.; Huang, C.; Zhang, Y. Regenerable CuO-Based Adsorbents for Low Temperature Desulfurization Application. *Ind. Eng. Chem. Res.* **2015**, *54*, 3556−3562.

(7) Shah, M. S.; Tsapatsis, M.; Siepmann, J. I. Hydrogen Sulfide Capture: From Absorption in Polar Liquids to Oxide, Zeolite, and Metal-Organic Framework Adsorbents and Membranes. *Chem. Rev.* **2017**, *117*, 9755−9803.

(8) Wang, X.; Sun, T.; Yang, J.; Zhao, L.; Jia, J. Low-Temperature H_2S Removal from Gas Streams with SBA-15 Supported ZnO Nanoparticles. *Chem. Eng. J.* **2008**, *142*, 48−55.

(9) Zhang, Q.; Lee, I.; Joo, J. B.; Zaera, F.; Yin, Y. Core−Shell Nanostructured Catalysts. *Acc. Chem. Res.* **2013**, *46*, 1816−1824.

(10) Chen, S.; Wei, Z.; Qi, X.; Dong, L.; Guo, Y.-G.; Wan, L.; Shao, Z.; Li, L. Nanostructured Polyaniline-Decorated Pt/C@PANI Core−Shell Catalyst with Enhanced Durability and Activity. *J. Am. Chem. Soc.* **2012**, *134*, 13252−13255.

(11) Bao, J.; He, J.; Zhang, Y.; Yoneyama, Y.; Tsubaki, N. A Core/Shell Catalyst Produces a Spatially Confined Effect and Shape Selectivity in a Consecutive Reaction. *Angew. Chem., Int. Ed.* **2008**, *47*, 353−356.

(12) Zhong, C. J.; Maye, M. M. Core−Shell Assembled Nanoparticles as Catalysts. *Adv. Mater.* **2001**, *13*, 1507−1511.

(13) Liu, S.; Zhang, N.; Xu, Y. J. Core-Shell Structured Nanocomposites for Photocatalytic Selective Organic Transformations. *Part. Part. Syst. Charact.* **2014**, *31*, 540−556.

(14) Yang, C.; Guo, W.; Cui, L.; An, N.; Zhang, T.; Guo, G.; Lin, H.; Qu, F. Fe_3O_4@$mSiO_2$ Core-Shell Nanocomposite Capped with Disulfide Gatekeepers for Enzyme-Sensitive Controlled Release of Anti-Cancer Drugs. *J. Mater. Chem. B* **2015**, *3*, 1010−1019.

(15) Kim, J.; Kim, H. S.; Lee, N.; Kim, T.; Kim, H.; Yu, T.; Song, I. C.; Moon, W. K.; Hyeon, T. Multifunctional Uniform Nanoparticles Composed of a Magnetite Nanocrystal Core and a Mesoporous Silica Shell for Magnetic Resonance and Fluorescence Imaging and for Drug Delivery. *Angew. Chem., Int. Ed.* **2008**, *47*, 8438−8441.

(16) Chen, Y.; Chen, H.; Zeng, D.; Tian, Y.; Chen, F.; Feng, J.; Shi, J. Core/Shell Structured Hollow Mesoporous Nanocapsules: A Potential Platform for Simultaneous Cell Imaging and Anticancer Drug Delivery. *ACS Nano* **2010**, *4*, 6001−6013.

(17) Wu, H.; Zhang, S.; Zhang, J.; Liu, G.; Shi, J.; Zhang, L.; Cui, X.; Ruan, M.; He, Q.; Bu, W. A Hollow-Core, Magnetic, and Mesoporous Double-Shell Nanostructure: In Situ Decomposition/Reduction Synthesis, Bioimaging, and Drug-Delivery Properties. *Adv. Funct. Mater.* **2011**, *21*, 1850−1862.

(18) Song, G.; Wang, Q.; Wang, Y.; Lv, G.; Li, C.; Zou, R.; Chen, Z.; Qin, Z.; Huo, K.; Hu, R.; Hu, J. A Low-Toxic Multifunctional Nanoplatform Based on Cu_9S_5@$mSiO_2$ Core-Shell Nanocomposites: Combining Photothermal- and Chemotherapies with Infrared Thermal Imaging for Cancer Treatment. *Adv. Funct. Mater.* **2013**, *23*, 4281−4292.

(19) Liu, X.; Ren, Q.; Fu, F.; Zou, R.; Wang, Q.; Xin, G.; Xiao, Z.; Huang, X.; Liu, Q.; Hu, J. CuS@$mSiO_2$-PEG Core-Shell Nanoparticles as a NIR Light Responsive Drug Delivery Nanoplatform for Efficient Chemo-Photothermal Therapy. *Dalton Trans.* **2015**, *44*, 10343−10351.

(20) Kou, T.; Wang, Y.; Zhang, C.; Sun, J.; Zhang, Z. Adsorption Behavior of Methyl Orange onto Nanoporous Core−Shell Cu@Cu_2O Nanocomposite. *Chem. Eng. J.* **2013**, *223*, 76−83.

(21) Tada, H.; Suzuki, F.; Ito, S.; Akita, T.; Tanaka, K.; Kawahara, T.; Kobayashi, H. Au-Core/Pt-Shell Bimetallic Cluster-Loaded TiO_2. 1. Adsorption of Organosulfur Compound. *J. Phys. Chem. B* **2002**, *106*, 8714−8720.

(22) Jiang, Z.; Xie, J.; Jiang, D.; Yan, Z.; Jing, J.; Liu, D. Enhanced Adsorption of Hydroxyl Contained/Anionic Dyes on Non Functionalized Ni@SiO_2 Core−Shell Nanoparticles: Kinetic and Thermodynamic Profile. *Appl. Surf. Sci.* **2014**, *292*, 301−310.

(23) Aslam, S.; Zeng, J.; Subhan, F.; Li, M.; Lyu, F.; Li, Y.; Yan, Z. In Situ One-Step Synthesis of Fe_3O_4@MIL-100(Fe) Core-Shells for Adsorption of Methylene Blue from Water. *J. Colloid Interface Sci.* **2017**, *505*, 186−195.

(24) Gui, C. X.; Li, Q. J.; Lv, L. L.; Qu, J.; Wang, Q. Q.; Hao, S. M.; Yu, Z. Z. Core-Shell Structured MgO@Mesoporous Silica Spheres for Enhanced Adsorption of Methylene Blue and Lead Ions. *RSC Adv.* **2015**, *5*, 20440−20445.

(25) Ghosh Chaudhuri, R.; Paria, S. Core/Shell Nanoparticles: Classes, Properties, Synthesis Mechanisms, Characterization, and Applications. *Chem. Rev.* **2012**, *112*, 2373−2433.

(26) He, Y. P.; Wang, S. Q.; Li, C. R.; Miao, Y. M.; Wu, Z. Y.; Zou, B. S. Synthesis and Characterization of Functionalized Silica-Coated Fe_3O_4 Superparamagnetic Nanocrystals for Biological Applications. *J. Phys. D: Appl. Phys.* **2005**, *38*, 1342−1350.

(27) Hu, J.-Q.; Meng, X.-M.; Jiang, Y.; Lee, C.-S.; Lee, S.-T. Fabrication of Germanium-Filled Silica Nanotubes and Aligned Silica Nanofibers. *Adv. Mater.* **2003**, *15*, 70−73.

(28) Gorelikov, I.; Matsuura, N. Single-Step Coating of Mesoporous Silica on Cetyltrimethyl Ammonium Bromide-Capped Nanoparticles. *Nano Lett.* **2008**, *8*, 369−373.

(29) Joo, S. H.; Park, J. Y.; Tsung, C. K.; Yamada, Y.; Yang, P.; Somorjai, G. A. Thermally Stable Pt/Mesoporous Silica Core-Shell Nanocatalysts for High-Temperature Reactions. *Nat. Mater.* **2009**, *8*, 126−131.

(30) Lee, I.; Zhang, Q.; Ge, J.; Yin, Y.; Zaera, F. Encapsulation of Supported Pt Nanoparticles with Mesoporous Silica for Increased Catalyst Stability. *Nano Res.* **2011**, *4*, 115−123.

(31) Chen, J.; Zhang, R.; Han, L.; Tu, B.; Zhao, D. One-Pot Synthesis of Thermally Stable Gold@mesoporous Silica Core-Shell Nanospheres with Catalytic Activity. *Nano Res.* **2013**, *6*, 871−879.

(32) Radloff, C.; Halas, N. J. Enhanced Thermal Stability of Silica-Encapsulated Metal Nanoshells. *Appl. Phys. Lett.* **2001**, *79*, 674−676.

(33) Zhang, X.; Wang, G.; Yang, M.; Luan, Y.; Dong, W.; Dang, R.; Gao, H.; Yu, J. Synthesis of a Fe_3O_4-CuO@meso-SiO_2 Nanostructure as a Magnetically Recyclable and Efficient Catalyst for Styrene Epoxidation. *Catal. Sci. Technol.* **2014**, *4*, 3082−3089.

(34) Yao, Q.; Lu, Z. H.; Zhang, Z.; Chen, X.; Lan, Y. One-Pot Synthesis of Core-Shell Cu@SiO_2 Nanospheres and Their Catalysis for Hydrolytic Dehydrogenation of Ammonia Borane and Hydrazine Borane. *Sci. Rep.* **2015**, *4*, 4−11.

(35) Ha, T.-L.; Kim, J. G.; Kim, S. M.; Lee, I. S. Reversible and Cyclical Transformations between Solid and Hollow Nanostructures in Confined Reactions of Manganese Oxide and Silica within Nanosized Spheres. *J. Am. Chem. Soc.* **2013**, *135*, 1378−1385.

(36) Zhou, W.; Zou, R.; Yang, X.; Huang, N.; Huang, J.; Liang, H.; Wang, J. Core-Decomposition-Facilitated Fabrication of Hollow Rare-Earth Silicate Nanowalnuts from Core-Shell Structures via the Kirkendall Effect. *Nanoscale* **2015**, *7*, 13715−13722.

(37) Lu, F.; Wang, J.; Yang, L.; Zhu, J. J. A Facile One-Pot Synthesis of Colloidal Stable, Monodisperse, Highly PEGylated CuS@$mSiO_2$ Nanocomposites for the Combination of Photothermal Therapy and Chemotherapy. *Chem. Commun.* **2015**, *51*, 9447−9450.

(38) Kang, X.; Cheng, Z.; Yang, D.; Ma, P.; Shang, M.; Peng, C.; Dai, Y.; Lin, J. Design and Synthesis of Multifunctional Drug Carriers

https://dx.doi.org/10.1021/acs.langmuir.0c00958
Langmuir 2020, 36, 6540−6549

Based on Luminescent Rattle-Type Mesoporous Silica Microspheres with a Thermosensitive Hydrogel as a Controlled Switch. *Adv. Funct. Mater.* **2012**, *22*, 1470−1481.
(39) Gates-Rector, S.; Blanton, T. The Powder Diffraction File: A Quality Materials Characterization Database. *Powder Diffr.* **2019**, *34*, 352−360.
(40) Kundu, J.; Pradhan, D. Influence of Precursor Concentration, Surfactant and Temperature on the Hydrothermal Synthesis of CuS: Structural, Thermal and Optical Properties. *New J. Chem.* **2013**, *37*, 1470−1478.
(41) Jiao, S.; Xu, L.; Jiang, K.; Xu, D. Well-Defined Non-Spherical Copper Sulfide Mesocages with Single-Crystalline Shells by Shape-Controlled Cu_2O Crystal Templating. *Adv. Mater.* **2006**, *18*, 1174−1177.
(42) Nakamura, R.; Tokozakura, D.; Nakajima, H.; Lee, J. G.; Mori, H. Hollow Oxide Formation by Oxidation of Al and Cu Nanoparticles. *J. Appl. Phys.* **2007**, *101*, 074303.
(43) Liu, J.; Xue, D. Thermal Oxidation Strategy towards Porous Metal Oxide Hollow Architectures. *Adv. Mater.* **2008**, *20*, 2622−2627.
(44) El Mel, A. A.; Nakamura, R.; Bittencourt, C. The Kirkendall Effect and Nanoscience: Hollow Nanospheres and Nanotubes. *Beilstein J. Nanotechnol.* **2015**, *6*, 1348−1361.
(45) Anderson, B. D.; Tracy, J. B. Nanoparticle Conversion Chemistry: Kirkendall Effect, Galvanic Exchange, and Anion Exchange. *Nanoscale* **2014**, *6*, 12195−12216.
(46) Yin, Y.; Rioux, R. M.; Erdonmez, C. K.; Hughes, S.; Somorjal, G. A.; Alivisatos, A. P. Formation of Hollow Nanocrystals Through the Nanoscale Kirkendall Effect. *Science* **2004**, *304*, 711−714.
(47) Birchenall, C. E. Diffusion in Sulfides. In *Geochemical Transport and Kinetics*; Paper presented at a conference at Airlie House, Warrenton, VA, June 1973; Hofmann, A. W., Giletti, B. J., Yoder, H. S., Jr., Yund, R. A., Eds.; Carnegie Institution of Washington: Washington DC, 1974; Publication 634, pp 54−59.
(48) Cassaignon, S.; Pauporté, T.; Guillemoles, J. F.; Vedel, J. Copper Diffusion in Copper Sulfide: A Systematic Study. *Ionics* **1998**, *4*, 364−371.
(49) Liu, X.; Mayer, M. T.; Wang, D. Understanding Ionic Vacancy Diffusion Growth of Cuprous Sulfide Nanowires. *Angew. Chem., Int. Ed.* **2010**, *49*, 3165−3168.
(50) Thermadam, S. P.; Bhagat, S. K.; Alford, T. L.; Sakaguchi, Y.; Kozicki, M. N.; Mitkova, M. Influence of Cu Diffusion Conditions on the Switching of Cu-SiO_2-Based Resistive Memory Devices. *Thin Solid Films* **2010**, *518*, 3293−3298.
(51) Nguyen, A. M.; Bahri, M.; Dreyfuss, S.; Moldovan, S.; Miche, A.; Méthivier, C.; Ersen, O.; Mézailles, N.; Carenco, S. Bimetallic Phosphide $(Ni,Cu)_2P$ Nanoparticles by Inward Phosphorus Migration and Outward Copper Migration. *Chem. Mater.* **2019**, *31*, 6124−6134.
(52) Basina, G.; Gaber, D. A.; Yafei, S. A.; Tzitzios, V.; Gaber, S. A.; Ismail, I.; Vaithilingam, B. V.; Polychronopoulou, K.; Hashimi, S. A.; Wahedi, Y. A. Mesoporous Silica "Plated" Copper Hydroxides/Oxides Heterostructures as Superior Regenerable Sorbents for Low Temperature H_2S Removal. *Chem. Eng. J.* **2020**, No. 125585.

https://dx.doi.org/10.1021/acs.langmuir.0c00958
Langmuir 2020, 36, 6540−6549